



Late Mio-Pliocene chemical weathering of the Yulong porphyry Cu deposit in the eastern Tibetan Plateau constrained by goethite (U–Th)/He dating: Implication for Asian summer monsoon



Xiao-Dong Deng^{a,b,c}, Jian-Wei Li^{a,*}, David L. Shuster^{b,c,*}

^a State Key Laboratory of Geological Processes and Mineral Resources, and Faculty of Earth Resources, China University of Geosciences, Wuhan 430074, China

^b Department of Earth and Planetary Science, University of California, Berkeley, CA 94720-4767, USA

^c Berkeley Geochronology Center, Berkeley, CA 94709, USA

ARTICLE INFO

Article history:

Received 11 October 2016

Received in revised form 20 April 2017

Accepted 23 April 2017

Available online 1 June 2017

Editor: D. Vance

Keywords:

chemical weathering

goethite

(U–Th)/He geochronology

monsoonal precipitation

southeastern Tibet

ABSTRACT

Chemical weathering has provided a potentially important feedback between tectonic forcing and climate evolution of the Asian continent, although precise constraints on the timing and history of weathering are only variably documented. Here, we use goethite (U–Th)/He and ⁴He/³He geochronology to constrain the timing and rates of chemical weathering at the Yulong porphyry Cu deposit on the eastern Tibetan Plateau. Goethite grains have (U–Th)/He ages ranging from 6.73 ± 0.51 to 0.53 ± 0.04 Ma that correlate with independent paleoclimatic proxies inferred from supergene Mn-oxides and loess deposits under variable tectonic regimes and vegetation zones over the southeastern Asia. This correlation indicates that regional climatic conditions, especially monsoonal precipitation, controlled chemical weathering and goethite precipitation in a vast area of southeastern Asia. The goethite ages suggest that the Asian summer monsoon was relatively strong from 7 to 4.6 Ma, but weakened between 4.6 and 4 Ma, and then significantly intensified from 4 to 2 Ma. The precipitation ages of goethites collected along a 100-m-thick weathering profile decrease with depth, and indicate a downward propagation of the weathering front at rates of <6.7, 53.5 ± 10.8, and 4.8 ± 0.6 m/Ma during the intervals of 7–4, 4–2, and 2–0.7 Ma, respectively. The rapid propagation of weathering front during 4–2 Ma was caused by abrupt lowering of the water table, which was possibly related to local surface uplift or reorganization of the river systems in southeastern Tibet during this period.

© 2017 Elsevier B.V. All rights reserved.

1. Introduction

Chemical weathering is important in shaping earth's surface and regulating global climate fluctuations and global chemical cycles. Precipitation, temperature, vegetation, and physical erosion are the dominant controls on long-term (>10⁶ yr) chemical weathering (White and Blum, 1995; Riebe et al., 2004; West et al., 2005). Identifying the primary controls on chemical weathering is important for understanding the interplay between tectonics and climate in the Asian continent (Molnar and England, 1990). Some authors have proposed that regional or local climate is the critical variable influencing chemical weathering (Clift et al., 2008), and others have emphasized that physical erosion, and a consequent supply of un-weathered materials, provides the primary control

on chemical weathering rates through time (Millot et al., 2002; Riebe et al., 2004).

Mineralogical, geochemical, and magnetic proxies from loess sections in the China Loess Plateau (An et al., 2005; Sun et al., 2010) and ocean sediments in the South China Sea (Wan et al., 2012; Clift et al., 2014) have been used to infer a record of chemical weathering over the Asian continent. However, changes in the provenance, and erosion and deposition rates of ocean sediments possibly complicate the interpretation of weathering proxies from marine sediments (Clift et al., 2014). In addition, chemical weathering indicators from loess deposits may be affected by the variation of eolian source and mass accumulation rates (Nie et al., 2014). Thus, the timing and history of chemical weathering in the Asian continent since the late Miocene remain controversial.

Weathering profiles can record a complex and protracted history of chemical and physical processes. Supergene minerals in weathering profiles commonly precipitate directly from weathering solutions, thus isotopic geochronology applied to these solids constrains the timing of chemical weathering processes

* Corresponding authors.

E-mail addresses: jwli@cug.edu.cn (J.-W. Li), dshuster@berkeley.edu (D.L. Shuster).

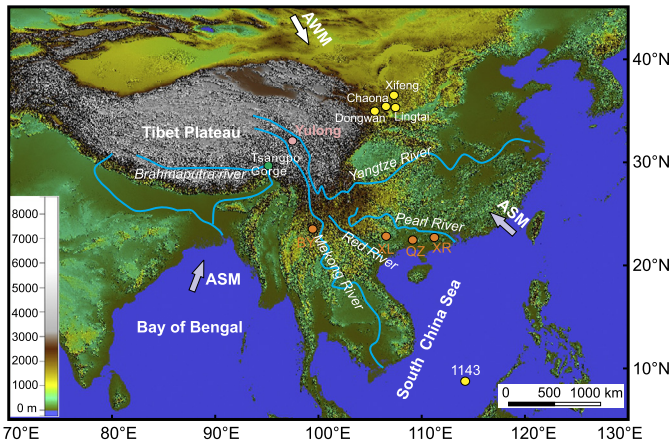


Fig. 1. Digital elevation map showing locations of the Yulong deposit, Lingtai–Chaona–Xifeng–Dongwan loess sections, Mn-oxide deposits from Yunnan Plateau (Baye – BY) and Southern China (Xialei – XL, Qinzhou – QZ, and Xinrong – XR), and ODP site 1143. AWM – Asian winter monsoon, ASM – Asian summer monsoon. Data are from the NASA Satellite Radar and Topography Mission (SRTM; <http://srtm.csi.cgiar.org/>).

(e.g., Beauvais et al., 2016; Bonnet et al., 2016). Supergene goethite forms mainly under relatively wet climate conditions (Tardy and Nahon, 1985), thus the frequency distribution of goethite ages can serve as a paleoclimatic proxy for past wet climatic conditions (Vasconcelos et al., 2015). Previous studies have demonstrated that goethite is suitable for (U–Th)/He dating; by using the $^4\text{He}/^3\text{He}$ methodology, loss of radiogenic ^4He by diffusion through the solid phase can be identified and accounted for to determine the timing of goethite precipitation (Shuster et al., 2005). Goethite (U–Th)/He and $^4\text{He}/^3\text{He}$ geochronology has been used to quantify rates of weathering front propagation (Heim et al., 2006), to determine formation ages of channel iron deposits (Vasconcelos et al., 2013), and to unravel changes of climatic conditions prevailing in the geological past (Vasconcelos et al., 2015).

Cenozoic porphyry Cu deposits are widely distributed over the Tibetan Plateau (Hou et al., 2003). Many of these deposits have been exposed to the surface or subsurface by post-mineralization exhumation processes, leading to prolonged oxidation of the mineralized porphyry and consequent formation of thick (~5–150 m) weathering profiles, which provide an ideal opportunity to determine the timing and history of chemical weathering and climatic conditions over the Tibetan Plateau. Here we present $^4\text{He}/^3\text{He}$ and (U–Th)/He dating results of supergene goethite from weathering profiles derived from the giant Yulong porphyry Cu deposit on the eastern Tibetan Plateau. These data are used to constrain the timing and duration of chemical weathering of regional significance. We further compare the observed goethite precipitation ages to time series of independent paleoclimatic proxies from the eastern margin of Tibetan Plateau and the South China block to document the fundamental controls on chemical weathering in southeastern Asia and to provide new insights into the Asian summer monsoon evolution since the late Miocene.

2. Geological background

The Yulong deposit (31°24′30″N, 97°44′00″E) in the eastern Tibetan Plateau (Fig. 1) is the third largest porphyry Cu deposit in China, with proven reserves of >6.2 Mt Cu and 0.4 Mt Mo (Hou et al., 2003). The ore-related granite porphyries have zircon U–Pb ages of 41.2–40.7 Ma, whereas molybdenite from Cu–Mo sulfide ores has a Re–Os isochron age of 40.1 ± 1.8 Ma (Hou et al., 2003). Copper mineralization occurred at ~2 km beneath the paleosurface (Tang, 2003), consisting mainly of quartz-sulfide stockworks and sulfide disseminations within altered porphyry intrusions, and stratiform Cu–Fe sulfide ores in the contact zones between the porphyries and late Triassic marine carbonate (Hou et al., 2003). Most orebodies have been brought to the surface or subsurface due to post-mineralization exhumation processes, resulting in oxidation of the primary sulfide ores and development of the thick weathering profiles in the Yulong deposit. Individual weathering profiles are 0–40 m thick in the north and 60–120 m in the south (Figs. 2 and 3) and contain a large variety of supergene Cu- and Fe-oxide

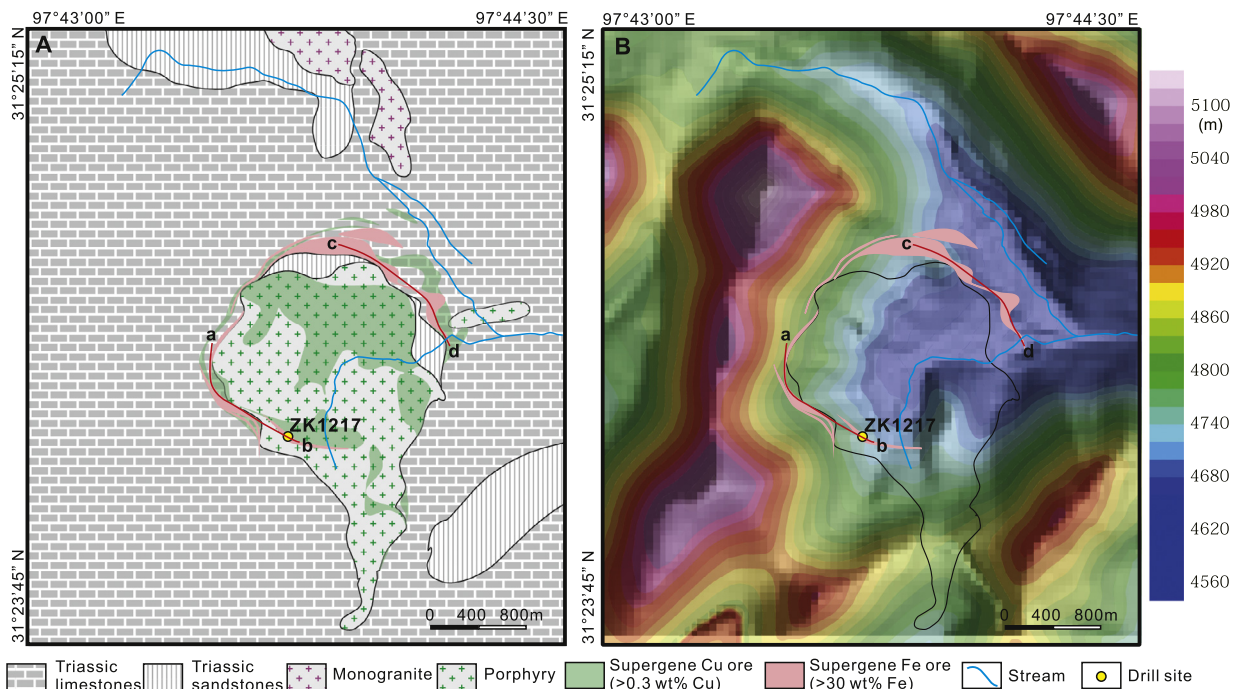


Fig. 2. (A) Geological map of the Yulong porphyry Cu deposit showing the occurrence of Fe-oxide and Cu orebodies and locations of two surface sections and one drill core. (B) Digital elevation map showing topography in the Yulong deposit.

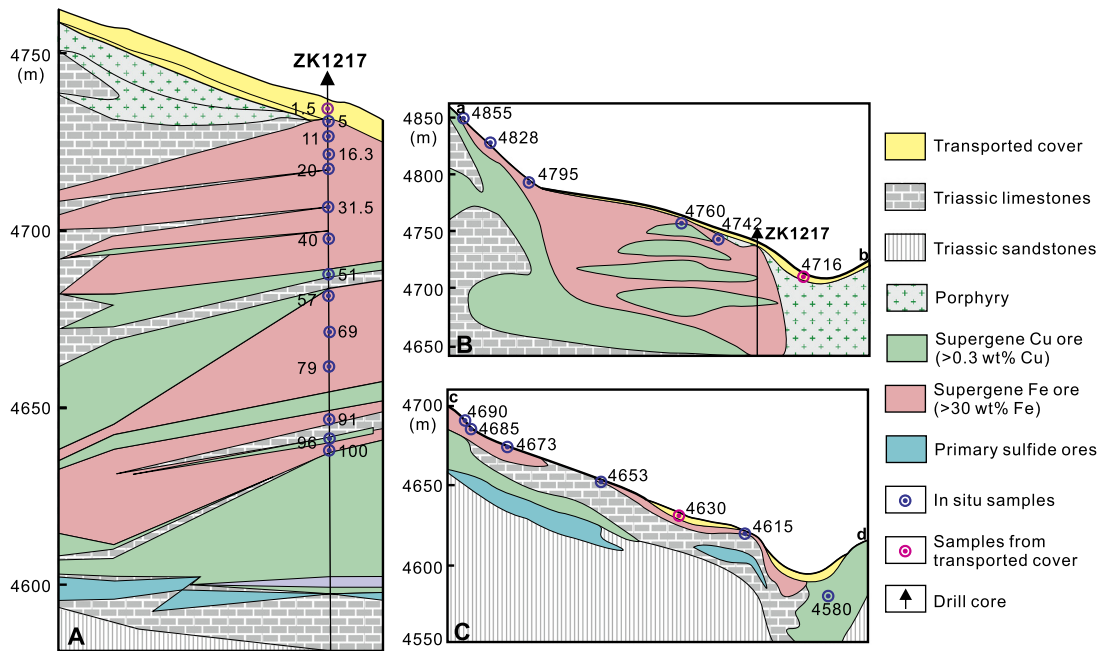


Fig. 3. (A) Stratigraphic column diagram showing the sampling location of ZK1217 drill core investigated in this study. The sample numbers represent the sampling depth. Geological cross-sections of a–b (B) and c–d (C) in the Yulong deposit showing the sampling locations of the surface samples in weathering profiles. The sample numbers represent the sampling elevation.

minerals of economic significance. Supergene iron oxides are particularly developed above the stratiform Cu–Fe orebodies, and are variably mantled by transported cover of 0–5 m thickness. Transported covers contain some iron oxide pebbles (Fig. 3), indicating the upper parts of weathering profiles on the hillslopes have been eroded or truncated by pediment.

The modern climate of the study area is dominated by a warm-wet summer monsoon in the summer and a cold-dry winter monsoon in the winter. The area typically receives 400–600 mm of annual precipitation, with a mean yearly evaporation of 1519 mm, and has a mean annual temperature of 8.1 °C (Table S1). The regional topography is characterized by a relatively low-relief surface (4500–5000 m elevation) bounded by the deeply incised Yangtze and Mekong rivers (Fig. 1), with regional base levels of ~4000 m. The low-relief surface has low erosion rates and has been interpreted as the product of in situ drainage reorganization (Yang et al., 2015) or the remnant of a past erosional surface (Clark et al., 2004). Topography of the mining area is characterized by hummocky hills that have moderate slope angles (15–40°) and have been variably dissected by NW- and EW-trending streams (Fig. 2B). Alluvial deposits along the streams are developed at 2–10 m above the beds of present stream channel. Currently, the water table decreases progressively from east to west in the mining area (Tang, 2003).

3. Sampling and methods

Twenty-six iron oxide samples were collected from a 100-m-deep drill core and two weathering sections well exposed by the open pit mining. Thirteen samples were collected from top to bottom of a single weathering profile revealed by drill hole ZK1217 (Fig. 3A). Five in-situ iron oxide samples were taken from the surface of weathering profiles along section a–b, and the sixth is an Fe-oxide pebble contained in transported cover overlying the weathering profile (Fig. 3B). Similarly, six in-situ iron oxide samples and one pebble were selected from the surface of weathering profiles along section c–d and the overlying transported cover (Fig. 3C), respectively. Goethites in all samples typically occur as

veins or cavity and fracture infilling (Fig. S1). They are generally of high purity and free from contaminants of hypogene phases (Figs. 4, 5), and thus are suitable for (U–He)/He dating.

Polished thin sections of each sample were examined under reflected-light and scanning electron microscopy to determine the mineral phases and paragenetic associations. Subsequently, pure goethite aliquots from individual samples were crushed, washed, and then dried at room temperature. For each sample, 50–100 grains (0.5 to 2 mm in diameter) of aggregated goethite crystallites were handpicked under a binocular microscope. The purity, composition, and crystallinity of goethite grains were further investigated by a combination of X-ray diffraction, electron microprobe, and scanning electron microscopy analyses.

Goethite (U–Th)/He and $^4\text{He}/^3\text{He}$ analyses were conducted at Berkeley Geochronology Center, and the experimental details and analytical protocols are summarized in Supplementary Materials. We use the $^4\text{He}/^3\text{He}$ release spectra of representative samples to estimate the proportion of ^4He lost by diffusion since goethite precipitation. The proportion of ^4He retained in each sample was quantified by dividing the bulk age of each by the apparent “plateau age” (Shuster and Farley, 2005). Then, we compared the corrected goethite (U–Th)/He ages to various paleoclimatic proxies using the t -test statistic to evaluate whether goethite precipitated preferentially under particular climatic conditions. We first plot the probability density patterns of goethite ages using different statistical methods. Probability Density Plots (PDP) are commonly used as an approximate of probability density, but they reduce the significance of imprecise ages and enhance the signals of precise ages (Vermeesch, 2012). Thus, a PDP produces a noisy age distribution for young goethite, and yields overly smoothed patterns for old goethite in this study (Fig. S3A). The Kernel Density Estimator (KDE) method has also been used to estimate the probability density (Vermeesch, 2012). A KDE plot of the observed goethite ages is consistent with their histogram and thus is suitable for estimating the probability density of weathering ages with variable uncertainties (Fig. S3). Thus, we create a synthetic dataset of both the supergene mineral ages and their probability from a KDE plot. Because paleoclimatic indicators and time-series of

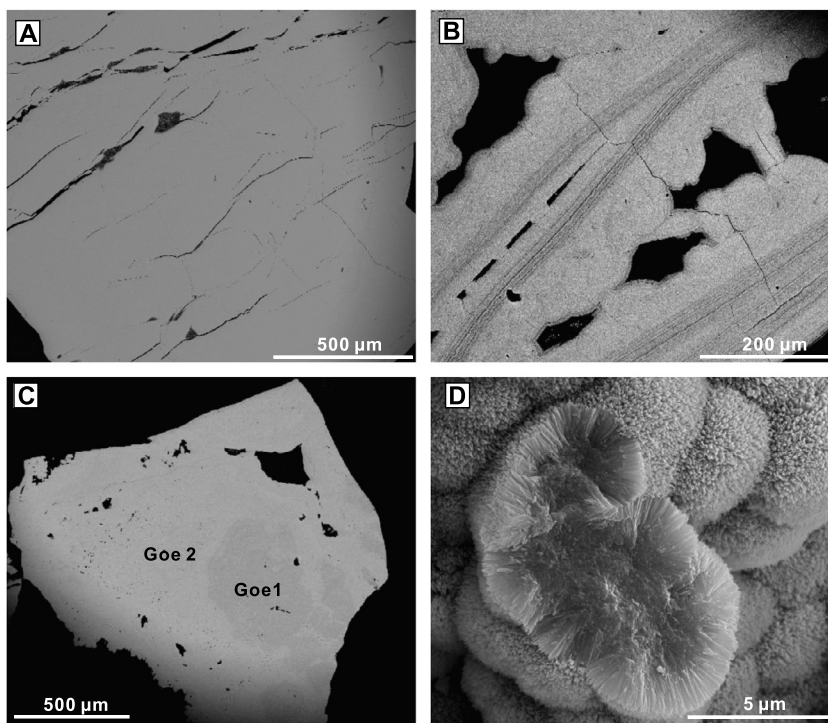


Fig. 4. Backscattered images of polished iron-oxide blocks show that this goethite has homogeneous texture (A), colloform texture of alternating growth bands (B), and multiple generations (C). Secondary electron image showing goethite occurring as aggregated, needle-like crystals (D).

loess deposits are determined, we can compare our goethite (U–Th)/He results to the independent paleoclimatic proxies using the *t*-test method following Riihimäki et al. (2009). The high absolute *t*-values (high positive *t* or low negative *t*) indicate strong correlations between the timing of goethite precipitation and climatic variations.

4. Results

Field observations confirm that iron-oxides investigated in this study formed by intensive weathering and oxidation of the primary Cu–Fe sulfides. Petrographic determinations show that goethite grains typically have massive, botryoidal, or banded textures, indicating direct precipitation from weathering solutions (Figs. 4 and S1). Most goethite grains have homogeneous texture (Fig. 4A), indicating a single episode of precipitation. Some grains consist of micrometric bands (Fig. 4B) or are characterized by multiple generations (Fig. 4C), indicating dissolution and re-precipitation. Secondary electron images reveal that goethite grains are composed of aggregated, needle-like crystals, with individual crystal being 0.1–2 μm long and <0.1 μm in diameter (Fig. 4D). X-ray diffraction patterns reveal intense and sharp peaks of goethite (Fig. S2), indicating relatively high crystallinity. Based on results of the peak width, goethite samples have mean crystal sizes between 13.3 and 29.4 nm (Fig. 5A). Electron microprobe analyses suggest that the goethite grains contain 76.06–91.73 wt% Fe₂O₃ (Fig. 5B), and 0.01–4.46 wt% Al₂O₃, with Al³⁺/(Fe³⁺+Al³⁺) molar ratios of 0.02–8.48% (Fig. 5C). The variations of Fe contents are likely due to the substitution or surface sorption of minor elements such as Al (Fig. 5C).

The goethite ⁴He/³He results are listed in Table S2. We use the ⁴He/³He release spectra of three representative samples (ZK1217-20, ZK1217-91 and 4673) to estimate the proportion of ⁴He lost by diffusion since goethite precipitation (Fig. 6). The “plateau ages” are defined by four or more continuous steps that contain radiogenic ⁴He gas released from homogeneous goethite

domains accounting for 38–61% of total ³He (Fig. 6). The minimum amount of released ³He used to calculate a “plateau age” depends on the components of high retentivity domains in goethite (Vasconcelos et al., 2013). All the three samples show ascending apparent ages at low release fractions (Fig. 6), indicating loss of ⁴He by diffusion since crystallization. The subsequent steps during middle to high temperatures yield invariant ⁴He/³He ages that we identify as “plateau ages”. The plateau segments have similar ⁴He/³He ratios in the three samples (Table S2), indicating that He was released at those steps from homogeneous goethite that quantitatively retained radiogenic ⁴He since crystallization (Vasconcelos et al., 2013). The last high-temperature steps (Fig. 6A and C) may reflect the presence of minor mineral contaminants that contain ⁴He not associated with goethite crystallization. We quantify the proportion of gas retained in each sample by dividing the observed bulk age of each by the “plateau ages” shown in Fig. 6. The proportions of ⁴He lost from samples ZK1217-20, ZK1217-91 and 4673 are 14.3%, 17.5% and 10.3%, respectively. The values of ⁴He diffusive loss in the three samples are inconsistent with the changes of mean crystal size (Fig. 5A). This observation indicates that a correction method based on crystallinity is unsuitable. Because three representative samples span the variance in age and crystallinity of all the investigated goethites (Fig. 5A), we assume that the mean of these proportions (and their variance) of ⁴He loss is applicable to all the analyzed samples. The mean value is 14.0% with uncertainty of 7.2% (2σ), indicating that ~86.0% of the ⁴He was retained within the solid. We thus divide the bulk (U–Th)/He ages of each of the other samples by the mean value of 86.0% to correct for diffusive loss of ⁴He according to the methods in Shuster et al. (2005). Although this is a necessary simplification, we estimate uncertainty in this correction by propagating uncertainties in the diffusive ⁴He loss fraction (7.2%) and the uncertainties in U, Th, Sm, and He measurements.

The corrected (U–Th)/He ages range from 6.73 ± 0.51 to 0.53 ± 0.04 Ma (2σ; Table S3). In most cases, different grains from

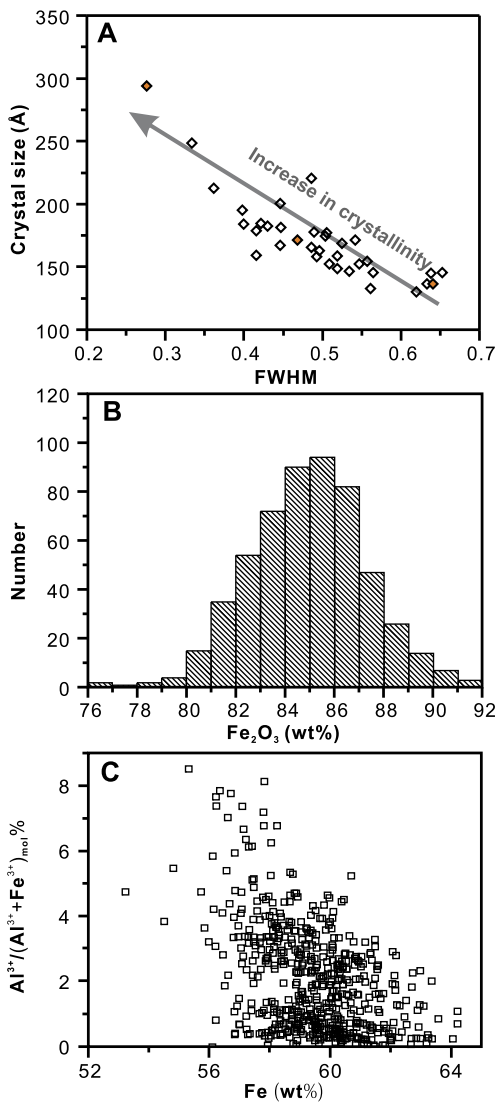


Fig. 5. (A) The relationship between FWHM (full width at half maximum intensity) of goethite peak at ca. 21.6° and crystal sizes estimated from powder X-ray diffraction patterns. Three orange diamonds are goethite samples used in $^4\text{He}/^3\text{He}$ analyses, indicating the decrease of crystallinity from ZK1217-20 to ZK1217-91 and 4673. (B) Histogram of Fe_2O_3 in goethite used for (U–Th)/He dating. (C) The negative correlation between Fe contents and $\text{Al}^{3+}/(\text{Fe}^{3+} + \text{Al}^{3+})$ molar ratios indicate Al substituted the Fe in structure of goethite.

individual samples yield reproducible ages, but several samples show large variance between aliquots (Fig. 7). Goethite samples from drill core ZK1217 show (U–Th)/He ages decrease with increasing depth beneath the surface (Fig. 7A), indicating a downward propagation of the weathering front through time. From these observations, propagation rates of weathering front are estimated to be 53.5 ± 10.8 and 4.8 ± 0.6 m/Ma during the intervals of 4–2 and 2–0.7 Ma, respectively (Fig. 7A). Goethite samples from the surface of weathering profiles along the two sections (Fig. 3B and C) show (U–Th)/He ages increase with decreasing elevations (Fig. 7B), suggesting the upper parts of weathering profiles have been progressively truncated by pediment. Statistical analyses (Table 1) reveal that the timing of goethite precipitation correlates with most time-variable paleoclimatic proxies, as indicated by the high absolute t -values (2.10–5.46) and low probability ($p < 0.05$).

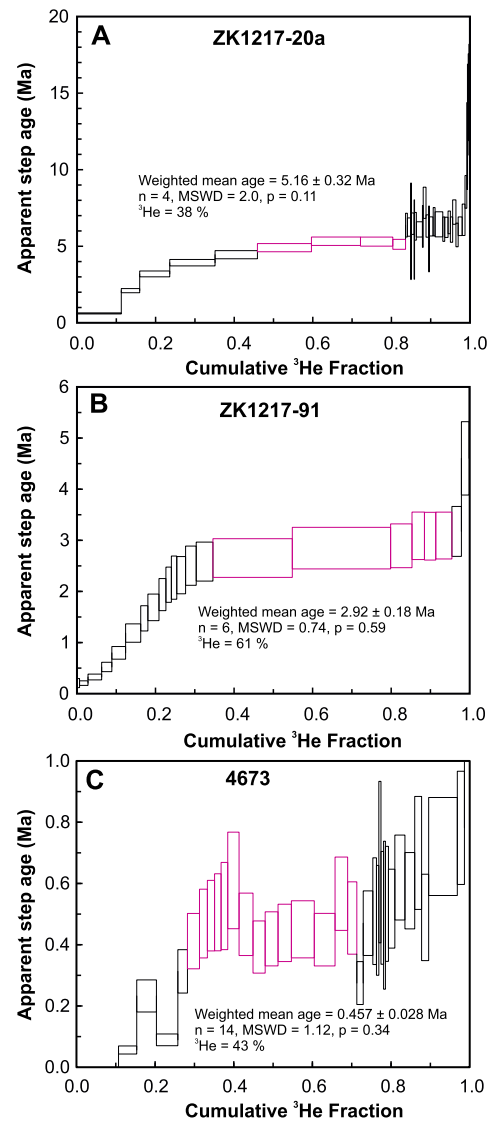


Fig. 6. Apparent step ages versus the cumulative release fraction of proton-induced ^3He for three representative samples [ZK1217-20 (A), ZK1217-91 (B), and 4673 (C)] analyzed using sequential degassing $^4\text{He}/^3\text{He}$ analysis.

5. Discussions

5.1. Caveats to the analysis and age data limitations

The goethite (U–Th)/He ages may be complicated, and their geological significance may be questionable, due to several potential problems: (1) ^4He loss from the iron-oxide structures due to diffusion (Shuster et al., 2005), (2) U and Th loss or gain from goethite by exchange with weathering solutions (Reiners et al., 2014); (3) contamination by other hypogene phases (Vasconcelos et al., 2013); and (4) multiple goethite generations present in a single grain (Monteiro et al., 2014). These potential problems, however, can be solved or avoided by using recently developed techniques with detailed petrographic investigation of goethite samples. $^4\text{He}/^3\text{He}$ methodology has proven capable of quantifying diffusive loss of radiogenic ^4He (Shuster and Farley, 2005; Shuster et al., 2005) and thus correcting the goethite (U–Th)/He ages (Fig. 6). In this study, different grains from an individual hand specimen, which typically have distinct U and Th concentrations, yield reproducible (U–Th)/He ages (Table S3). This internal reproducibility strongly suggests that U and Th exchanges with weathering solutions did not pose problems in accurately dating

Table 1

t-test analysis of the correlation between climate proxies and goethite (U–Th)/He ages.

Paleoclimate proxy	t value mean	t value SD	p	Data number	Time interval (Ma)
Mn-oxides ages of Yunnan Plateau ^[1]	5.18	0.55	<0.0001	62	0–7 Ma
Mn-oxides ages of Southern China ^[2,3]	3.7	0.58	0.0013	63	0–7 Ma
Loess MS from Lingtai ^[4]	5.46	0.88	0.0001	3370	0–7 Ma
Summer monsoon stack from loess ^[4]	5.21	0.94	0.0001	5046	0–7 Ma
Normalized silicate weathering rate of ODP1143 ^[5]	2.1	0.2	0.0441	51	0–5 Ma

^[1]Deng et al. (2014); ^[2]Li et al. (2007a, 2007b); ^[3]Yan (2006); ^[4]Sun et al. (2010); ^[5]Wan et al. (2012).

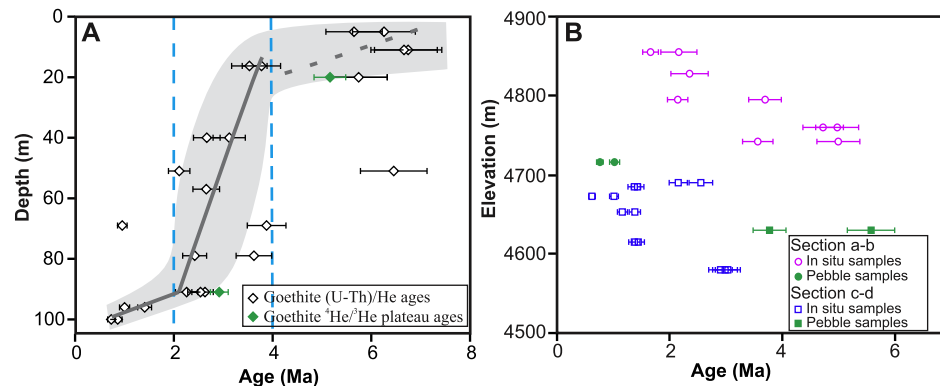


Fig. 7. (A) Depth profile of goethite (U–Th)/He ages from drill core (ZK1217) in the Yulong deposit. Linear regression curves (solid line) indicate downward propagation rates of weathering front at 53.5 ± 10.8 m/Ma ($y = -53.5x + 210.1$; $R = -0.88$) during 4–2 Ma and 4.8 ± 0.6 m/Ma ($y = -4.8x + 102.8$; $R = -0.95$) during 2–0.7 Ma. Gray areas represent 95% confidence band of linear fit. (B) (U–Th)/He ages of the observed goethite samples from the surface of two weathering sections in the Yulong deposit negatively correlate with sampling elevations. All the points represent the corrected (U–Th)/He ages and uncertainties for individual aliquots. (For interpretation of the references to color in this figure legend, the reader is referred to the web version of this article.)

our goethite. An integration of petrographic characterization, X-ray diffraction, scanning electron microscopy, and electron microprobe analysis indicates that the goethite grains investigated in this study are pure and do not contain any hypogene phases (Figs. 4 and 5). Therefore, the (U–Th)/He dates can be reliably interpreted as the precipitation ages of goethite. Textural evidence revealed presence of multiple goethite generations in a single grain (Fig. 4C), presumably caused by dissolution and re-precipitation processes. In this case, different aliquots from such grains may yield variable (U–Th)/He ages (Fig. 7). Therefore, detailed petrographic determination and strict sampling strategy must be exercised to avoid multiple goethite generations in the grains used for (U–Th)/He dating.

Detailed sampling along the vertical extent of a weathering profile is key to understand the complete weathering history. On the one hand, supergene goethites at greater depths in weathering profiles may be inaccessible. Thus, geochronological information on the most recent weathering process is unlikely to be retrieved. Fortunately, the drill cores have allowed us to collect goethite samples from the lowest part of weathering profiles in the Yulong deposit (Fig. 3A), which yielded the youngest (U–Th)/He age of 0.73 Ma and record the latest weathering history at Yulong (Fig. 7A). On the other hand, the oldest supergene minerals at the top of weathering profiles could be removed away, leading to incomplete records of the early weathering history. Although weathering profiles from the Yulong deposit were variably eroded (Fig. 3), the drill core (ZK1217) and iron-oxide pebbles demonstrate that goethite samples from some upper zones of the weathering profiles have been preserved, and can record the complete weathering history since ca. 7 Ma (Fig. 7).

Another important limitation in the interpretation of chemical weathering based on KDE plots of weathering ages is whether the age data quantity is sufficiently large to adequately represent the complete weathering signals extracted from the (U–Th)/He age data. The age probability density of the observed goethite is coincident with the chemical weathering indicators from supergene

Mn-oxides, loess, and marine sediments in southeastern Asia since ~7 Ma (Fig. 8). This consistency suggests that the number of goethite (U–Th)/He ages is sufficient to determine the long-term weathering history. Further studies on O and H isotopes of supergene minerals (e.g., Yapp and Shuster, 2011) in these weathering profiles may provide better understanding in chemical weathering history.

5.2. Rates of weathering front propagation

Goethite precipitated directly from weathering solutions at or close to the weathering front. Thus, goethite (U–Th)/He ages can be regarded as a function of precipitation depth and provide useful information on the rates of weathering front propagation (Heim et al., 2006). Goethite (U–Th)/He ages from a 100-m-thick weathering profile at Yulong progressively decrease with increasing depth (Fig. 7A), indicating continuous lowering of weathering fronts since ~7 Ma. In the upper part of the weathering profile (≤ 20 m), however, goethite (U–Th)/He ages are poorly correlated with depth, possibly due to dissolution and re-precipitation of goethite occurring at the surface or subsurface prior to ca. 4 Ma (Monteiro et al., 2014). This also suggests that the observed goethites remained stable in the weathering system since ca. 4 Ma (Fig. 7), otherwise their U, Th, and He isotopic systematics would have been reset by later weathering events. In this case, the (U–Th)/He results indicate that goethite in the upper part of weathering profile formed since at least ca. 7 to 4 Ma, and thus an upper limit on the weathering front propagation rate (6.7 m/Ma) can be estimated by using the time interval and depth of the goethite samples from the weathering profile. In the lower part of weathering profile (>20 m), the correlation between goethite age and sample depth yields a higher value of 53.5 ± 10.8 m/Ma between 4 and 2 Ma, and a lower rate of 4.8 ± 0.6 m/Ma after 2 Ma (Fig. 7A). The lower rates are consistent with values calculated using $^{40}\text{Ar}/^{39}\text{Ar}$ ages of supergene Mn-oxides from lateritic profiles in south Yunnan plateau since

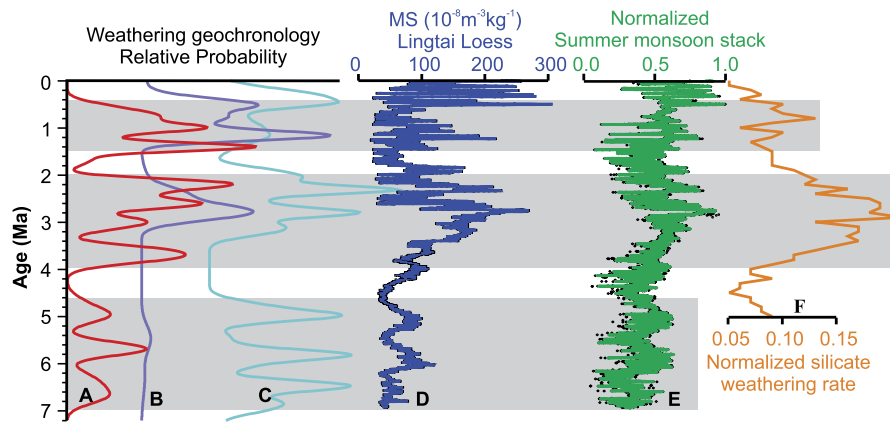


Fig. 8. Time series showing correlations between goethite precipitation ages and various paleoclimatic proxies. (A) KDE plots for goethite (U–Th)/He ages (corrected for diffusive loss of ^4He ; Table S3) from the Yulong deposit. (B) KDE plots for Mn-oxides ages from Yunnan Plateau (Deng et al., 2014). (C) KDE plots for Mn-oxides ages from South China (Yan, 2006; Li et al., 2007a, 2007b). (D) Magnetic susceptibility (MS) of loess sediments from Lingtai section (Sun et al., 2010). (E) Normalized summer monsoon stack indicator from Lingtai loess section (Sun et al., 2010). (F) Normalized silicate weathering rate from ODP1143 (Wan et al., 2012).

~ 3 Ma (3.3–11.1 m/Ma; Deng et al., 2014) and in Guizhou plateau for the past 13.1 Ma (3.3 m/Ma; Deng et al., 2016).

The unusually high rate of weathering front propagation from 4 to 2 Ma (Fig. 7) can be interpreted as the abrupt lowering of water table due to climate desiccation, surface uplift, or reorganizing the river courses. Continuous aridity causes a progressive lowering of the water table through time, thus leading to a downward propagation of the weathering front and consequent precipitation of goethite near the water table (Heim et al., 2006). This scenario, however, is not supported by the extensive lateritic weathering and other paleoclimatic proxies over southeastern Asia that reveal a wetter climate induced by strengthening of Asian summer monsoon during 4–2 Ma (Fig. 8). As such, the rapid propagation of weathering front during this period cannot be ascribed to an arid climatic condition. Alternatively, surface uplift in this region may have caused rapid downward movement of water table and thus lowering of the weathering front. However, stable isotope paleoaltimetry results suggest that the southeastern margin of Tibetan Plateau reached its present altitude in the late Eocene (Hoke et al., 2014), arguing against significant surface uplift between 4 and 2 Ma. Nevertheless, local surface uplift may be related to the movement of numerous faults on the southeastern margin of Tibetan Plateau. This is confirmed by local surface uplift may occur along the left-lateral/normal Litang fault system since Pliocene (Zhang et al., 2015) and the left-lateral/thrusting Selaha and Zheduotang faults since ~ 4 Ma (Zhang et al., 2017). Thus, the rapid lowering of weathering front during 4–2 Ma is possibly caused by local surface uplift due to the movement of Tuoba and Wenquan strike-slip faults in the Yulong region (Hou et al., 2003). Lastly, the lowering of water table in this region may have been caused by drainage reorganization over the southeastern margin of Tibetan Plateau since the late Miocene (Yang et al., 2015). Although drainage reorganization may mainly occur before the late Miocene in this region (Clark et al., 2004), recent studies reveal that reorganization and incision of the deep gorges draining the southeastern margin of Tibetan Plateau are likely related to the northward movement of the Indian continent corner since the late Miocene (Yang et al., 2016). This view is supported by incision in the headwaters of the Red River during the late Pliocene (Fig. 1; Schoenbohm et al., 2004) and rapid incision of the Tsangpo Gorge at 2.5–2 Ma (Fig. 1; Wang et al., 2014). The incision of the deep gorges may propagate outward to affect regional streams, as illustrated by the well-developed alluvium deposits above the beds of active stream channels in and around the Yulong mine. The lowering of stream channels by incision can promote water drainage from hills to the western streams (Fig. 2B), facilitating downward

movement of the water table on hillslopes. Collectively, we propose that the rapid downward propagation of the weathering front during 4–2 Ma is likely driven by local surface uplift or drainage reorganization in this region.

5.3. Insights into late Mio-Pliocene monsoonal precipitation

The results of *t*-tests (Table 1) show that the probability distribution of goethite precipitation ages in the Yulong deposit correlates with that of supergene Mn-oxides from lateritic profiles in the Yunnan Plateau and South China (Fig. 8A–C), indicating pervasive chemical weathering in southeastern Asia since ca. 7 Ma. The primary controls on this prolonged regional chemical weathering remain controversial.

Previous studies reveal that precipitation, temperature, vegetation, and tectonics are all possible factors affecting chemical weathering (e.g., White and Blum, 1995; West et al., 2005). As temperature increases, chemical reaction rates increase, resulting in higher weathering rates (White and Blum, 1995). Since the late Miocene, a decreasing temperature trend has been revealed from the benthic foraminifera $\delta^{18}\text{O}$ in South China Sea (Wang et al., 2003) and magnetic parameters of loess deposits in NW China (Nie et al., 2014). This decrease is consistent with the persistent global cooling since the late Miocene (Zachos et al., 2001). The distribution pattern of goethite (U–Th)/He ages combined with other chemical weathering proxies over southeastern Asia (Fig. 8) indicate significantly enhanced chemical weathering during 4–2 Ma. This contradicts the persistent cooling trend since the late Miocene, suggesting that temperature did not exert a dominant control on the chemical weathering in this region.

Vegetation plays an important role in increasing permeability of weathered materials, lowering pH value of weathering solutions by release of CO_2 and organic acids, and thus enhancing chemical weathering (Drever, 1994). Weathering proxies from variable vegetation types, such as highland meadow/steppe region (goethite in the Yulong region), temperate steppe zone (loess sections in China Loess Plateau), and tropical–subtropical forest regions (Mn-oxides deposits in South China), are all well correlated with each other. Meanwhile, palaeobotanical records suggest that vegetation zones in those regions have been sustained since the late Miocene (Sun and Wang, 2005). Therefore, similar chemical weathering histories in those regions preclude vegetation as a dominant factor controlling the chemical weathering in southeastern Asia.

Numerous studies have emphasized that exposure of unweathered rocks by physical erosion can promote chemical weathering, and thus a correlation should exist between the chemical

weathering and erosion rates (Millot et al., 2002; Riebe et al., 2004; West et al., 2005). Weathering geochronology of supergene Fe- and Mn-oxides has suggested that the pre-late Miocene supergene minerals in the eastern Tibetan Plateau (this study) and Yunnan Plateau (Deng et al., 2014) have been largely eroded due to relatively active tectonism; whereas the early to middle Miocene Mn-oxides remain well preserved in South China which is characterized by tectonic quiescence (Li et al., 2007a, 2007b). This contrast suggests progressive increase in physical erosion toward areas proximal to the eastern Tibetan Plateau (Deng et al., 2016). However, KDE plots of the supergene mineral ages from those regions extending for >1600 km are well correlated each other (Fig. 8A–C). This correlation contradicts the progressive changes of physical erosion rates in the regions, suggesting that physical erosion is not a significant control on the chemical weathering in southeastern Asia.

Goethite precipitation requires water to dissolve sulfide minerals and to transport ferric ions. Increased rainfall brings more abundant oxygenated water to facilitate chemical weathering and goethite precipitation from the weathering solutions. Meanwhile, previous studies demonstrated that an increase in precipitation over the Asian continent is caused by strengthening of the Asian summer monsoon (e.g., An et al., 2005; Clift et al., 2014), resulting in enhanced chemical weathering. Therefore, goethite formation at Yulong is most likely related to the changes of monsoonal precipitation. Magnetic susceptibility of loess deposits is a robust indicator for chemical weathering and Asian monsoon evolution (An et al., 2005; Sun et al., 2010). As the Asian summer monsoon strengthens, rainfall and chemical weathering rates increase, facilitating formation of pedogenic magnetic minerals (e.g., magnetite and maghemite) and consequently increasing in magnetic susceptibility of loess deposits (An et al., 2005). Our goethite (U–Th)/He ages correlate well with magnetic susceptibility of loess deposits from the Lingtai section (Table 1; Fig. 8D; Sun et al., 2010), suggesting a possible causal link between goethite precipitation and Asian summer monsoon strengthening since ~7 Ma. The stacked Asian summer monsoon index (Fig. 8E), which is a combination of magnetic susceptibility and carbonate content from the Lingtai section (Sun et al., 2010), also correlates with the goethite (U–Th)/He ages, further confirming a link between the monsoonal precipitation and goethite formation.

5.4. Implications for late Mio-Pliocene Asian summer monsoon evolution

Numerous studies of the loess deposits and lacustrine sediments in southeastern Asia have well established the history and evolution of Asian summer monsoon during the Quaternary (e.g., An et al., 2011). However, the late Miocene to Pliocene evolution of Asian summer monsoon remains poorly understood (An et al., 2005; Passey et al., 2009; Clift et al., 2014). Our goethite (U–Th)/He ages suggest that the Asian summer monsoon was relatively strong between 7 and 4.6 Ma and was significantly intensified at 4–2 Ma. In contrast, we observe essentially no goethite precipitation between 4.6 and 4 Ma, likely suggesting dry condition due to weakening of the Asian summer monsoon during this period.

As for the 7–4.6 Ma interval, whether the Asian summer monsoon is relatively strong (Passey et al., 2009; Nie et al., 2014) or weak (An et al., 2005; Clift et al., 2008) has long been debated. The fine-grained nature of all observed goethites (Fig. 5A) suggests a wet climatic condition since goethite precipitation, otherwise the precipitated goethite will be completely replaced with hematite (Langmuir, 1971; Tardy and Nahon, 1985). According to thermodynamic data of Al-substitution in goethite (Tardy and Nahon, 1985), the low-Al goethite in the Yulong deposit likely formed at a high activity of water (Fig. 5C), indicating a wet climate that

is related to relatively strong Asian summer monsoon during this period. This view is also supported by prevailing precipitation of supergene Mn-oxides in subtropical South China during 7–5 Ma (Fig. 8B and C), which has been linked to the intensification of the Asian summer monsoon (Li et al., 2007a). Independent proxies from red clay sequences over China Loess Plateau also suggest a relatively strong Asian summer monsoon during the late Miocene to early Pliocene (Ding et al., 2001). The high clay coatings, dark Fe–Mn films, and arboreal components in red clay sequences over China Loess Plateau suggest a relatively strong Asian summer monsoon during the late Miocene to early Pliocene (Ding et al., 2001; Ma et al., 2005; Wang et al., 2006). Temperature and precipitation variations inferred from magnetic parameters of red clay indicate relatively strong Asian summer monsoon during 6–4.8 Ma (Nie et al., 2014).

During 4.6–4 Ma, the lack of goethite precipitation is either due to inadequate sampling or a hiatus of chemical weathering. Our sampling strategy consists of representative samples from a drill core and two weathering sections spanning the entire oxidation zone of the Yulong deposit both horizontally and vertically (Fig. 3), thus inadequate sampling is an unlikely scenario. The lack of goethite formation during 4.6–4 Ma corresponds well to the lack of Mn-oxides precipitation in the South China and Yunnan Plateau during the same period (Fig. 8A–C). These lack of supergene Fe- and Mn-oxides across a vast area of southeastern Asia may be best interpreted in terms of a waning stage of chemical weathering during this period. This large-scale weakening of chemical weathering can be linked to a weakened Asian summer monsoon that caused climatic desiccation in southeastern Asia. This view is supported by the low mean annual precipitation estimated from magnetic parameters of the red clay sequences at Chaona and Lingtai during 4.8–4.3 Ma (Nie et al., 2014). Pollen assemblages at 4.5–3.7 Ma in Xifeng section show arboreal pollens decrease from 27% to 12%, whereas drought-tolerant species (*Ephedra* and *Chenopodiaceae*) suddenly increase from 8.1% to 21% (Wang et al., 2006). This trend documents prevailing aridity during 4.5 to 3.7 Ma, likely due to the weakening Asian summer monsoon. Recent mollusks studies have revealed that three arid species (*Cathaica pulveraticula*, *Cathaica schensiensis*, *Pupopsis retrodens*) are only identified in Dongwan loess section at 4.4–3.5 Ma (Li et al., 2014), confirming the suggestion of arid climate and relatively weak Asian summer monsoon during this period.

During 4–2 Ma, the frequency of goethite (U–Th)/He ages coincides with a rapid downward propagation of the weathering front (Figs. 7, 8A), indicating high chemical weathering rates during this period. This consideration is consistent with the high probabilities of Mn-oxides from lateritic weathering profiles throughout South China and Yunnan plateau during 3.6–2 Ma (Fig. 8B and C), indicating a wetter period caused by intensification of Asian summer monsoon in southeastern Asia. This view is supported by high normalized chemical weathering rates at 4–2 Ma (Fig. 8F, Wan et al., 2012) inferred from ocean sediments in South China Sea. An intensified Asian summer monsoon is also reflected in paleoclimatic proxies from the loess deposits in China Loess Plateau, including relatively high magnetic susceptibility (Fig. 8D; An et al., 2005) and stacked summer monsoon index (Fig. 8E; Sun et al., 2010) at 3.6–2.4 Ma.

6. Conclusions

Goethites from weathering profiles in the Yulong porphyry Cu deposit in the eastern Tibetan Plateau yield (U–Th)/He ages between 6.73 and 0.53 Ma. Climatic conditions inferred from these goethite ages are consistent with variation in paleoclimatic conditions deduced from supergene Mn-oxides and loess deposits in southeastern Asia. The observed goethite (U–Th)/He ages sug-

gest monsoonal precipitation controlled the chemical weathering in southeastern Asia, and further reveal a relatively strong Asian summer monsoon from 7–4.6 and 4–2 Ma, but a weak monsoon from 4.6–4 Ma. Goethite ages obtained from a ~100 m drill core systematically decrease with increasing depth, and yield an unusually high rate of weathering front propagation during 4–2 Ma. This rapid lowering of weathering front was possibly related to local surface uplift or drainage reorganization in this region that caused the lowering of water table at this period. Our results confirm that goethite (U–Th)/He geochronology is a robust approach for determining the timing and history of chemical weathering and paleoclimatic evolution of regional significance.

Acknowledgements

We thank Nick Fylstra, Jia Chang and Shentai Liu, and Hongqiang Wang for their help during (U–Th)/He analysis, field work, and sample preparation, respectively. This work was jointly supported by the National Natural Science Foundation of China (41325007), the Ann and Gordon Getty Foundation, and International Postdoctoral Exchange Fellowship Program from China Postdoctoral Science Foundation (2013–81), and National Demonstration Center for Experimental Mineral Exploration Education at China University of Geosciences (Wuhan).

Appendix A. Supplementary material

Supplementary material related to this article can be found online at <http://dx.doi.org/10.1016/j.epsl.2017.04.043>.

References

- An, Z., Clemens, S.C., Shen, J., Qiang, X., Jin, Z., Sun, Y., Prell, W.L., Luo, J., Wang, S., Xu, H., Cai, Y., Zhou, W., Liu, X., Liu, W., Shi, Z., Yan, L., Xiao, X., Chang, H., Wu, F., Ai, L., Lu, F., 2011. Glacial–interglacial Indian summer monsoon dynamics. *Science* 333, 719–723.
- An, Z., Huang, Y., Liu, W., Guo, Z., Clemens, S., Li, L., Prell, W., Ning, Y., Cai, Y., Zhou, W., Lin, B., Zhang, Q., Cao, Y., Qiang, X., Chang, H., Wu, Z., 2005. Multiple expansions of C_4 plant biomass in East Asia since 7 Ma coupled with strengthened monsoon circulation. *Geology* 33, 705–708.
- Beauvais, A., Bonnet, N.J., Chardon, D., Arnaud, N., Jayananda, M., 2016. Very long-term stability of passive margin escarpment constrained by $^{40}\text{Ar}/^{39}\text{Ar}$ dating of K–Mn oxides. *Geology* 44, 299–302.
- Bonnet, N.J., Beauvais, A., Arnaud, N., Chardon, D., Jayananda, M., 2016. Cenozoic lateritic weathering and erosion history of Peninsular India from $^{40}\text{Ar}/^{39}\text{Ar}$ dating of supergene K–Mn oxides. *Chem. Geol.* 446, 33–53.
- Clark, M.K., Schoenbohm, L.M., Royden, L.H., Whipple, K.X., Burchfiel, B.C., Zhang, X., Tang, W., Wang, E., Chen, L., 2004. Surface uplift, tectonics, and erosion of eastern Tibet from large-scale drainage patterns. *Tectonics* 23, TC1006.
- Clift, P.D., Hodges, K.V., Heslop, D., Hannigan, R., Van Long, H., Calves, G., 2008. Correlation of Himalayan exhumation rates and Asian monsoon intensity. *Nat. Geosci.* 1, 875–880.
- Clift, P.D., Wan, S., Blusztajn, J., 2014. Reconstructing chemical weathering, physical erosion and monsoon intensity since 25 Ma in the northern South China Sea: a review of competing proxies. *Earth-Sci. Rev.* 130, 86–102.
- Deng, X.-D., Li, J.-W., Vasconcelos, P.M., Cohen, B.E., Kusky, T.M., 2014. Geochronology of the Baye Mn oxide deposit, southern Yunnan Plateau: implications for the late Miocene to Pleistocene paleoclimatic conditions and topographic evolution. *Geochim. Cosmochim. Acta* 139, 227–247.
- Deng, X.-D., Li, J.-W., Vasconcelos, P.M., 2016. $^{40}\text{Ar}/^{39}\text{Ar}$ dating of supergene Mn-oxides from the Zunyi Mn deposit, Guizhou Plateau, SW China: implications for chemical weathering and paleoclimatic evolution since the late Miocene. *Chem. Geol.* 445, 185–198.
- Ding, Z., Yang, S., Sun, J., Liu, T., 2001. Iron geochemistry of loess and red clay deposits in the Chinese Loess Plateau and implications for long-term Asian monsoon evolution in the last 7.0 Ma. *Earth Planet. Sci. Lett.* 185, 99–109.
- Drever, J.L., 1994. The effect of land plants on weathering rates of silicate minerals. *Geochim. Cosmochim. Acta* 58, 2325–2332.
- Heim, J.A., Vasconcelos, P.M., Shuster, D.L., Farley, K.A., Broadbent, G., 2006. Dating paleochannel iron ore by (U–Th)/He analysis of supergene goethite, Hamersley province, Australia. *Geology* 34, 173–176.
- Hoke, G.D., Liu, Z.J., Hren, M.T., Wissink, G.K., Garzzone, C.N., 2014. Stable isotopes reveal high southeast Tibetan Plateau margin since the Paleogene. *Earth Planet. Sci. Lett.* 394, 270–278.
- Hou, Z., Ma, H., Zaw, K., Zhang, Y., Wang, M., Wang, Z., Pan, G., Tang, R., 2003. The Himalayan Yulong porphyry copper belt: product of large-scale strike-slip faulting in eastern Tibet. *Econ. Geol.* 98, 125–145.
- Langmuir, D., 1971. Particle size effect on the reaction goethite=hematite+water. *Am. J. Sci.* 271, 147–156.
- Li, F., Wu, N., Rousseau, D.-D., Dong, Y., Zhang, D., Pei, Y., 2014. Late Miocene–Pliocene paleoclimatic evolution documented by terrestrial mollusk populations in the Western Chinese Loess Plateau. *PLoS ONE* 9, e95754.
- Li, J.-W., Vasconcelos, P., Duzgoren-Aydin, N., Yan, D.-R., Zhang, W., Deng, X.-D., Zhao, X.-F., Zeng, Z.-P., Hu, M.-A., 2007a. Neogene weathering and supergene manganese enrichment in subtropical South China: an $^{40}\text{Ar}/^{39}\text{Ar}$ approach and paleoclimatic significance. *Earth Planet. Sci. Lett.* 256, 389–402.
- Li, J.-W., Vasconcelos, P., Zhang, W., Deng, X.-D., Duzgoren-Aydin, N., Yan, D.-R., Zhang, J.-Q., Hu, M.-A., 2007b. Timing and duration of supergene mineralization at the Xinrong manganese deposit, western Guangdong Province, South China: cryptomelane $^{40}\text{Ar}/^{39}\text{Ar}$ dating. *Miner. Depos.* 42, 361–383.
- Ma, Y., Wu, F., Fang, X., Li, J., An, Z., Wang, W., 2005. Pollen record from red clay sequence in the central Loess Plateau between 8.10 and 2.60 Ma. *Chin. Sci. Bull.* 50, 2234–2243.
- Millot, R., Gaillardet, J., Dupré, B., Allègre, C.J., 2002. The global control of silicate weathering rates and the coupling with physical erosion: new insights from rivers of the Canadian Shield. *Earth Planet. Sci. Lett.* 196, 83–98.
- Molnar, P., England, P., 1990. Late Cenozoic uplift of mountain ranges and global climate change: chicken or egg? *Nature* 346, 29–34.
- Monteiro, H.S., Vasconcelos, P.M., Farley, K.A., Spier, C.A., Mello, C.L., 2014. (U–Th)/He geochronology of goethite and the origin and evolution of cangas. *Geochim. Cosmochim. Acta* 131, 267–289.
- Nie, J., Stevens, T., Song, Y., King, J.W., Zhang, R., Ji, S., Gong, L., Cares, D., 2014. Pacific freshening drives Pliocene cooling and Asian monsoon intensification. *Sci. Rep.* 4, 5474.
- Passey, B.H., Ayliffe, L.K., Kaakinen, A., Zhang, Z., Eronen, J.T., Zhu, Y., Zhou, L., Cerling, T.E., Fortelius, M., 2009. Strengthened East Asian summer monsoons during a period of high-latitude warmth? Isotopic evidence from Mio–Pliocene fossil mammals and soil carbonates from northern China. *Earth Planet. Sci. Lett.* 277, 443–452.
- Reiners, P.W., Chan, M.A., Evenson, N.S., 2014. (U–Th)/He geochronology and chemical composition of diagenetic cement, concretions, and fracture-filling oxide minerals in Mesozoic sandstones of the Colorado Plateau. *Geol. Soc. Am. Bull.* 126, 1363–1383.
- Riebe, C.S., Kirchner, J.W., Finkel, R.C., 2004. Erosional and climatic effects on long-term chemical weathering rates in granitic landscapes spanning diverse climate regimes. *Earth Planet. Sci. Lett.* 224, 547–562.
- Riihimaki, C.A., Reiners, P.W., Heffern, E.L., 2009. Climate control on Quaternary coal fires and landscape evolution, Powder River basin, Wyoming and Montana. *Geology* 37, 255–258.
- Schoenbohm, L.M., Whipple, K.X., Burchfiel, B.C., Chen, L., 2004. Geomorphic constraints on surface uplift, exhumation, and plateau growth in the Red River region, Yunnan Province, China. *Geol. Soc. Am. Bull.* 116, 895–909.
- Shuster, D.L., Farley, K.A., 2005. $^4\text{He}/^3\text{He}$ thermochronometry: theory, practice, and potential complications. *Rev. Mineral. Geochem.* 58, 181–203.
- Shuster, D.L., Vasconcelos, P.M., Heim, J.A., Farley, K.A., 2005. Weathering geochronology by (U–Th)/He dating of goethite. *Geochim. Cosmochim. Acta* 69, 659–673.
- Sun, Y., An, Z., Clemens, S.C., Bloemendal, J., Vandenberghe, J., 2010. Seven million years of wind and precipitation variability on the Chinese Loess Plateau. *Earth Planet. Sci. Lett.* 297, 525–535.
- Sun, X., Wang, P., 2005. How old is the Asian monsoon system?—Palaeobotanical records from China. *Palaeogeogr. Palaeoclimatol. Palaeoecol.* 222, 181–222.
- Tang, J.X., 2003. The Study on Metallogeny and Localizing Forecast of Yulong Porphyry Copper–Molybdenum Mineralization, Xizang (Tibet). Ph.D. thesis. China University of Geoscience, Beijing, 270 pp.
- Tardy, Y., Nahon, D., 1985. Geochemistry of laterites, stability of Al-goethite, Al-hematite, and Fe^{3+} -kaolinite in bauxites and ferricretes: an approach to the mechanism of concretion formation. *Am. J. Sci.* 285, 865–903.
- Vasconcelos, P.M., Heim, J.A., Farley, K.A., Monteiro, H., Waltenberg, K., 2013. $^{40}\text{Ar}/^{39}\text{Ar}$ and (U–Th)/He– $^4\text{He}/^3\text{He}$ geochronology of landscape evolution and channel iron deposit genesis at Lynn Peak, Western Australia. *Geochim. Cosmochim. Acta* 117, 283–312.
- Vasconcelos, P.M., Reich, M., Shuster, D.L., 2015. The paleoclimatic signatures of supergene metal deposits. *Elements* 11, 317–322.
- Vermeesch, P., 2012. On the visualisation of detrital age distributions. *Chem. Geol.* 312–313, 190–194.
- Wan, S., Clift, P.D., Li, A., Yu, Z., Li, T., Hu, D., 2012. Tectonic and climatic controls on long-term silicate weathering in Asia since 5 Ma. *Geophys. Res. Lett.* 39, L15611.
- Wang, L., Lü, H.Y., Wu, N.Q., Li, J., Pei, Y.P., Tong, G.B., Peng, S.Z., 2006. Palynological evidence for Late Miocene–Pliocene vegetation evolution recorded in the red clay sequence of the central Chinese Loess Plateau and implication for palaeoenvironmental change. *Palaeogeogr. Palaeoclimatol. Palaeoecol.* 241, 118–128.
- Wang, P., Scherler, D., Liu-Zeng, J., Mey, J., Avouac, J.-P., Zhang, Y., Shi, D., 2014. Tectonic control of Yarlung Tsangpo Gorge revealed by a buried canyon in Southern Tibet. *Science* 346, 978–981.

- Wang, P., Zhao, Q., Jian, Z., Cheng, X., Huang, W., Tian, J., Wang, J., Li, Q., Li, B., Su, X., 2003. Thirty million year deep sea records in the South China Sea. *Chin. Sci. Bull.* 48, 2524–2535.
- West, A.J., Galy, A., Bickle, M., 2005. Tectonic and climatic controls on silicate weathering. *Earth Planet. Sci. Lett.* 235, 211–228.
- White, A.F., Blum, A.E., 1995. Effects of climate on chemical weathering in watersheds. *Geochim. Cosmochim. Acta* 59, 1729–1747.
- Yan, D.R., 2006. Metallogenetic Epoch and Genesis of Supergene Manganese Deposits in Xialei, SW Guangxi (Southern China). Master thesis. China University of Geoscience. 73 p.
- Yang, R., Fellin, M.G., Herman, F., Willett, S.D., Wang, W., Maden, C., 2016. Spatial and temporal pattern of erosion in the Three Rivers Region, southeastern Tibet. *Earth Planet. Sci. Lett.* 433, 10–20.
- Yang, R., Willett, S.D., Goren, L., 2015. In situ low-relief landscape formation as a result of river network disruption. *Nature* 520, 526–529.
- Yapp, C.J., Shuster, D.L., 2011. Environmental memory and a possible seasonal bias in the stable isotope composition of (U–Th)/He-dated goethite from the Canadian Arctic. *Geochim. Cosmochim. Acta* 75, 4194–4215.
- Zachos, J., Pagani, M., Sloan, L., Thomas, E., Billups, K., 2001. Trends, rhythms, and aberrations in global climate 65 Ma to present. *Science* 292, 686–693.
- Zhang, Y.-Z., Replumaz, A., Leloup, P.H., Wang, G.-C., Bernet, M., van der Beek, P., Paquette, J.L., Chevalier, M.-L., 2017. Cooling history of the Gongga batholith: implications for the Xianshuihe Fault and Miocene kinematics of SE Tibet. *Earth Planet. Sci. Lett.* 465, 1–15.
- Zhang, Y.-Z., Replumaz, A., Wang, G.-C., Leloup, P.H., Gautheron, C., Bernet, M., van der Beek, P., Paquette, J.L., Wang, A., Zhang, K.-X., Chevalier, M.-L., Li, H.-B., 2015. Timing and rate of exhumation along the Litang fault system, implication for fault reorganization in Southeast Tibet. *Tectonics* 34, 1219–1243.